Proceedings of the 2000 IEEE
International Conference on Robotics & Automation
San Francisco, CA • April 2000

Kinematic Transformations for Remotely-Actuated Planar Continuum Robots

Ian A. Gravagne and Ian D. Walker
Dept. of Electrical and Computer Engineering, Clemson University, Clemson, SC
igravag@ces.clemson.edu, ianw@ces.clemson.edu

Abstract

In this work, we consider a class of robotic manipulators generally termed "hyper-redundant". Specifically, we seek to examine some of the kinematic properties of "continuum" hyper-redundant robots. Unlike the case with rigid-link robots, there is no commonly accepted formula for describing continuum robot kinematics. Although these manipulators are continuously flexible, they are actuated with a finite number of actuators. In this paper, we discuss two possible options for mapping desired infinite-dimensional robot shapes to the finite-dimensional actuator space, using "natural" and "wavelet" decompositions. We compare and contrast these kinematic descriptions, illustrating how the wavelet decomposition can simplify the inverse kinematics for redundant planar continuum robots.

1 Introduction

Traditionally, rigid-link manipulators have dominated the robotics community commensurate with their domination of the natural world. Rigid-link systems provide the vast majority of locomotive and manipulative needs, at least on dry land. However, alternative methods of manipulation and locomotion based on very high-degree-of-freedom backbones ("HDOF" robots), such as snakes, or continuous trunks and tentacles ("continuum" robots), offer some advantages. These manipulators, generally termed "hyper-redundant", exhibit unique capabilities which render them extraordinarily useful in cluttered or unstructured environments, or where exceptionally fine and detailed manipulation is required. Hyper-redundant manipulators have the potential to accomplish tasks beyond the realm of traditional rigid-link manipulators, including the ability to suffer localized damage without paralyzing subsequent operation. Certain classes of hyper-redundant manipulators, such as the ones considered in this paper, possess *inherent compliance* which allows them to safely contact their environment and conform to it without the use of highly complex and expensive force feedback schemes.

Unfortunately, very few hyper-redundant (HDOF or continuum) robots exist yet. Because researchers have not yet mastered the intricacies of their construction and use, much more work must be done to perfect our understanding of how to model, control, build and successfully use them. Toward these ends, several researchers have worked in the area of hyper-redundant robots for manipulation and locomotion. In Japan, Hirose pioneered the development of snake-like robots, especially with regards to locomotion; an overview of his work exists in [1]. Also, Mochiyama, et. al., have investigated the problem of controlling the shape of an HDOF rigid-link robot with two-degree-of-freedom joints using spatial curves [6]-[8]. For robots possessing continuous back-bones, a good overview exists in [15]. These authors plus Suzumori, et. al., in [16] have done significant work in flexible hydraulic micro-actuators for grippers, which are essentially small, flexible, 3-DOF manipulators. The primary body of work upon which we draw is that of Chirikjian and Burdick, [9]-[13], who laid the foundations for the kinematic theory of hyper-redundant robots. In this paper, we build upon

Figure 1: The Elephant's Trunk.

work with the Rice/Clemson Elephant's Trunk (a type of HDOF remotely-actuated manipulator [2], see figure 1), as well as basic kinematic theory for remotely-actuated continuum robots in general [3]. Similar to the Elephant's Trunk but much larger in scale is the commercially manufactured GreyPilgrim "EMMA" serpentine manipulator [4].

2 Background

At the heart of the problems surrounding the study of hyper-redundant robots is the question of "shape control", in other words, what shape the robot should take at any point in time. One possibility utilizes a virtual robot, whose (greatly simplified) kinematics reflect only enough information to generate the appropriate spatial curves for the task at hand. The virtual robot moves and evolves in response to whatever shape-optimization and path-planning techniques are employed to generate its backbone curve. A "fitting algorithm" then attempts to match a real, rigid-link robot to the virtual backbone curve as closely as possible (the definition of "close" being key to the discussion). The fitting method is fundamental to the foundational works of Chirikjian and Burdick [9]-[13], who used variable geometry truss platforms for their real robots, and also Mochiyama et. al. [6]-[8].

However, one of the primary assumptions in the fitting method requires perfect knowledge (at least kinematically) of the real robot. In this paper, we consider robots which are themselves continuous curves (or which, like the Elephant's Trunk, possess a high number of rigid links, many of which are passive). While one may perfectly control the shape of a virtual continuum robot, real robots still require the use of actuators such as motors which necessarily act to apply force or torque to a finite number of points on the robot structure, through cables or tendons in the case of remote actuation. Thus it is inevitable that the (infinite-dimensional) continuous backbone will assume a particular pose based not only upon the (finite number of) motor inputs, but also upon external physical forces such as gravity or objects in the environment, as well as minimum potential energy principles.

Unfortunately, this very observation serves to limit the usefulness of any kinematic continuum robot model. In fact, even with a precise knowledge and model of the robot itself (stiffness profile of the backbone, effects of gravity, friction on the tendons, etc.), inherent compliance ruins any chance of knowing exactly "where the robot is" using only tendon-length feedback without direct sensing of some variety. Obtaining such a model would lead one into the depths of such fields as beam theory, and it is not clear that the result of all the effort would necessarily yield a formulation significantly more useful than a simpler model, given that such factors as unmodeled effects, ill-modeled effects, imperfect parametric knowledge and inherent compliance will always lurk in the background.

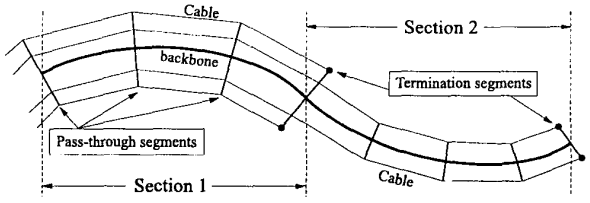

Figure 2: A 2-section planar manipulator. In the plane, each section is 1-DOF.

So it seems prudent to sprinkle a healthy dose of engineering judgement onto the kinematic modeling efforts, to arrive at a mathematical foundation which reflects a "high enough" degree of reality and usefulness without drowning the new and exciting aspects of continuum robots in a quagmire of complexity and details. This is part of the challenge that hyper-redundant robots offer in general, over and above the requirements of traditional rigid-link robots.

In [3], we explore one possibility for describing the kinematics of "multi-section", continuum, remotely-actuated robots such as the Elephant's Trunk and similar prototype robots in our laboratory. These robots are characterized by a flexible backbone which is not allowed to twist. Perpendicular spacers periodically attached to the backbone serve either to guide cables down the backbone (called pass-through segments) or to allow the cables to exert forces on the backbone (called termination segments). The length between two termination segments is termed a section, and sections are the basic building blocks of remotely-actuated continuum robots. In the plane, a section possesses one pair of opposing cables and has 1-DOF; in space a section needs two (orthogonally positioned) pairs of cables which make it a 2-DOF manipulator. Sections are attached in series to form a whole manipulator, and [3] explores the details of modeling a section and how changes in cable lengths affect the bending in a section. Figure 2 illustrates a 2-section planar robot.

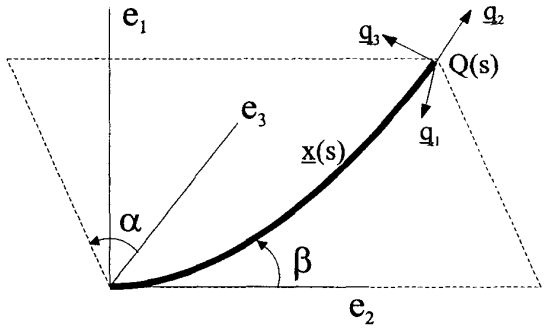

Figure 3: An illustration of the angles in a continuum manipulator section.

3 Single-Section Kinematics

In the absence of external forces each section would ideally bend only in a plane. In order to capture this observation, the picture in figure 3 was adopted. Here, the particular plane in which the backbone bends is chosen by the angle α, and the bending angle itself is reflected in the function $\beta(s)$. The variable s is a dimensionless independent parameter, usually varying between 0 to 1. We fix $\beta(0) = 0$ and expect the backbone to lie in a straight line along the e_2 axis unless the cables pull on it. There is a "moving frame" $Q(s)$ which describes the orientation of the backbone at any point along its length, and a related position vector $\underline{x}(s)$, where

$$\begin{aligned} Q(s) &= \begin{bmatrix} c_\alpha^2 + s_\alpha^2 c_\beta & s_\alpha s_\beta & -c_\alpha s_\alpha(1-c_\beta) \\ -s_\alpha s_\beta & c_\beta & -c_\alpha s_\beta \\ -c_\alpha s_\alpha(1-c_\beta) & c_\alpha s_\beta & s_\alpha^2 + c_\alpha^2 c_\beta \end{bmatrix} \\ \underline{x}(s) &= \int_0^s \underline{q}_2(\sigma)d\sigma, \end{aligned} \tag{1}$$

$c_\alpha = \cos\alpha$, $s_\alpha = \sin\alpha$, etc. The second column of Q is $\underline{q}_2(s)$, the tangent vector to the backbone. Because the backbone does not extend or contract, s reflects the backbone arc-length. In general, forces such as gravity will pull backbone sections out of the plane, and we must then consider $\alpha(s)$ as a variable along with $\beta(s)$.

The frame $Q(s)$ for one section contains three distinct rotations,

$$Q = [R_{e_2,\alpha}][R_{e_1,\beta}][R_{e_2,-\alpha}], \tag{2}$$

where $R_{e_2,\alpha}$ symbolizes a "rotation about axis e_2 of α radians". Clearly, if $\beta(s) = 0$, the backbone lies in a straight line with $Q(s) = I_{3\times 3}$. This is its "minimum energy" configuration. Extending this principle, we can arrive at differential system for $\alpha(s)$ and $\beta(s)$ which describes the backbone curve in a minimum energy fashion in general, where the cable lengths provide final conditions on the system. If we assign a weighting function $w(s)$ to reflect the local "bendability" of the backbone, and a gravitational potential energy function $gh(\alpha(s), \beta(s))$, then we obtain

$$\begin{aligned} \ddot{\alpha}(1-\cos\beta) &= \frac{g}{2w}\frac{\partial h}{\partial \alpha} - \frac{\dot{w}}{w}\dot{\alpha}(1-\cos\beta) - \dot{\alpha}\dot{\beta}(\sin\beta) \\ \ddot{\beta} &= \frac{g}{w}\frac{\partial h}{\partial \beta} - \frac{\dot{w}}{w}\dot{\beta} + \dot{\alpha}^2(\sin\beta) \end{aligned} \tag{3}$$

where $\dot{\alpha} = \frac{d\alpha(s)}{ds}$, etc. Initial and final conditions are

$$\begin{aligned} \beta(0) &= 0 \qquad \beta(1) = \frac{1}{a}\sqrt{\Delta L_{ca}{}^2 + \Delta L_{cb}{}^2} \\ \alpha(0) &= \tan^{-1}\left(\frac{\Delta L_{ca}}{\Delta L_{cb}}\right) \qquad \dot{\alpha}(0) = 0, \end{aligned} \tag{4}$$

which is to say, we model $\alpha(s)$ as remaining constant (even though it might not if $\frac{g}{w}$ is too large), with the initial condition on $\alpha(s)$ and the final condition on $\beta(s)$ determined by parameters related to the change in cable lengths (see [3] for details).

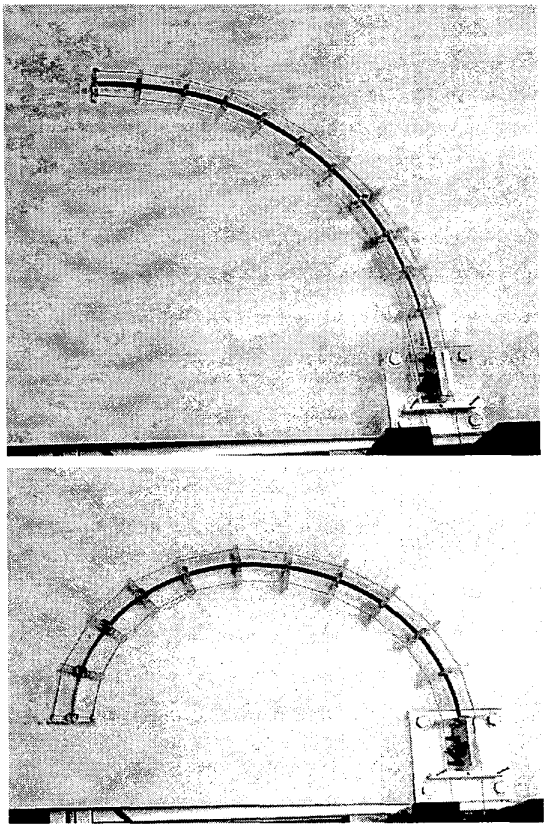

Figure 4: One section of a continuum robot bends into semi-circles. The backbone material is a piece of "spring" steel.

Even with our simplified view of the flexible backbone, this set of differential equations is complex enough to contain a singularity at $\beta(s) = 0$ which makes it very difficult to work with. Rather than attempting to elucidate all of the detail contained in (3), we consider in this paper the planar case. There, $\alpha(s)$ remains fixed (say, at 0 or $\pi/2$) by design, and there are no gravitational effects with which to contend. In this case, we simply have

$$\begin{aligned} \ddot{\beta} &= 0 \\ \beta(0) &= 0 \qquad \beta(1) = \frac{\Delta L_{ca}}{a}, \end{aligned} \tag{5}$$

where ΔL_{ca} is the change in cable length bending the backbone out of a straight line, and a is the distance from the backbone to the cables. The system can be re-written with two initial conditions

$$\beta(0) = 0 \qquad \dot{\beta}(0) = \mu \tag{6}$$

where μ is constant, so the solution is simply linear, i.e. $\beta(s) = \mu s$. (Here $\mu = \frac{\Delta L_{ca}}{a}$, but we will soon release the constraint that a section must be unit length, which changes the manner in which the initial condition relates

to the final condition.) This solution corresponds to the ideal semicircular arc of radius $\frac{1}{\mu}$, as illustrated in figure 4.

4 The Natural Basis Functions

We now concern ourselves with connecting several sections together in series. Essentially, we can see the overall kinematic structure by multiplying several section frames, from (2),

$$\begin{aligned} Q(s) &= [R_{e_2,\alpha_1}][R_{e_1,\beta_1}][R_{e_2,\alpha_2-\alpha_1}][R_{e_1,\beta_2}][R_{e_2,\alpha_3-\alpha_2}] \\ &\quad \cdots [R_{e_2,\alpha_n-\alpha_{n-1}}][R_{e_1,\beta_n}][R_{e_2,-\alpha_n}] \end{aligned} \quad (7)$$

where we have attached n sections together. In general, the complete description in (7) is cumbersome and unwieldy, though quite similar in that respect to traditional rigid-link robots. However, in the plane, a simplification appears by noting that all α_i are equal and constant. In this manner (7) collapses to

$$Q(s) = [R_{e_2,\alpha}][R_{e_1,\beta_1+\beta_2+\ldots+\beta n}][R_{e_2,-\alpha}]. \quad (8)$$

We denote the summation $\beta_1(s) + \beta_2(s) + \ldots + \beta_n(s) \triangleq \beta_T(s)$. As discussed earlier, if the bending affinity $w(s)$ remains constant over a section, that section will exhibit linear $\beta_i(s)$, which means $\beta_T(s)$ will appear to have n linear sections, with (11) implying $\beta_T(s)$ must be continuous. Now we note that the robot's planar position is

$$\underline{x}(s) = \begin{bmatrix} \int_0^s \sin\beta_T(\sigma)d\sigma \\ \int_0^s \cos\beta_T(\sigma)d\sigma \end{bmatrix} \quad (9)$$

for a non-extensible backbone. Now the position and orientation are functions of $\beta_i(s)$ for $i = 1..n$, which must be computed for each section. Setting the robot's total backbone length to unity, we may divide the robot into n sections. We "sample" the total arc length at points s_0, s_1, s_2,..., s_n, note that $s_0 = 0$, $s_n = 1$, and define the "i^{th}" section as that where $s \in [s_{i-1}, s_i]$. (For simplicity, we assume the s_i are evenly spaced, so $s_i - s_{i-1} = \frac{1}{n}$.) Then, $\beta_i(s)$ has the general form

$$\beta_i(s) = \left\{ \begin{array}{ll} 0 & s < s_{i-1} \\ \beta_T(s) - \beta_T(s_{i-1}) & s_{i-1} \le s \le s_i \\ \beta_T(s_i) & s > s_i \end{array} \right\}. \quad (10)$$

Note that these functions vary only on $s \in [s_{i-1}, s_i]$, and remain constant before and after that interval. The variable portion, $\beta(s)$, obeys the rules for a section from (5). A modification must be made to the initial conditions so that

$$\beta_i(s_{i-1}) = \beta_{i-1}(s_{i-1}) \qquad \dot{\beta}_i(s_{i-1}) = \mu_i \quad (11)$$

and $\beta_1(0) = 0$.

Owing to the initial conditions on β_i in (11), we also note that

$$\dot{\beta}_T(s) = \frac{1}{\sqrt{n}} \sum_{i=1}^{n} \mu_i \phi_i^b(s). \quad (12)$$

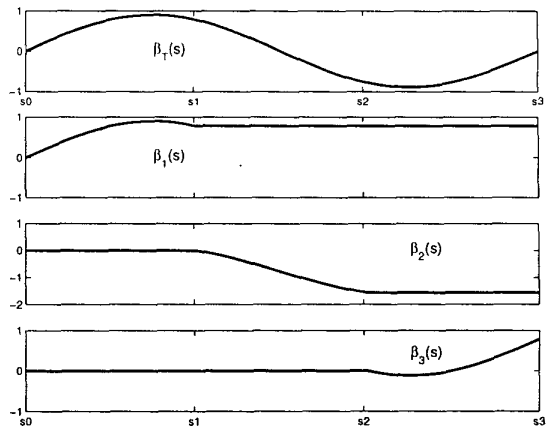

Figure 5: An example of how the function $\beta_T(s)$ is composed of $\beta_1(s) + \beta_2(s) + \beta_3(s)$.

where $\phi_i^b(s)$ is the simple "box" function

$$\phi_i^b(s) = \left\{ \begin{array}{ll} \sqrt{n}, & s \in [s_{i-1}, s_i] \\ 0 & otherwise \end{array} \right\}. \quad (13)$$

Integrating (12),

$$\beta_T(s) = \frac{1}{\sqrt{n}} \sum_{i=1}^{n} \mu_i \Phi_i^b(s), \qquad \Phi_i(s) = \int_0^1 \phi_i^b(\sigma)d\sigma \quad (14)$$

which can be written $\beta_T(s) = \frac{1}{\sqrt{n}} \underline{\mu}^T \underline{\Phi}^b(s)$. After substituting (14) back into the position formula, we may finally obtain the equations of motion by differentiating with respect to time,

$$\frac{d\underline{x}(s)}{dt} = \frac{d\underline{x}(s)}{d\underline{\mu}} \frac{d\underline{\mu}}{dt} \triangleq \left[J(\underline{\mu}, s)\right] \frac{d\underline{\mu}}{dt} \quad (15)$$

where $J_{1,i} = \int_0^s \Phi_i^b(\sigma) \cos\left(\underline{\mu}^T \underline{\Phi}^b(\sigma)\right) d\sigma$ and $J_{2,i} = -\int_0^s \Phi_i^b(\sigma) \sin\left(\underline{\mu}^T \underline{\Phi}^b(\sigma)\right) d\sigma$. If only the end-effector motions are of concern, then Jacobian $J \in \Re^{2\times n}$, and the upper limit on the integrals is $s = 1$. However, if the robot consists of sufficiently numerous sections, then (15) may account for additional points along the robot's length up until J is square.

5 The Wavelet Basis Functions

Fundamentally, the decomposition in (12) represents a mapping from the space of infinite-dimensional real-valued functions to the finite-dimensional space $\Re^n$. Intuitively, this is necessary because, while the backbone curve may be able to assume an infinite spectrum of shapes, the finite number of actuators available cannot achieve but a small subset of those. The basis functions, $\phi_i^b(s)$, were chosen because they naturally fit the problem

at hand, and we term them the "natural basis functions". Once the mapping is complete, the distinct and independent μ_i provide a direct physical link back to the robot actuators, via expressions for tendon lengths explored in [3]. This is a type of "modal decomposition", as explored in [9], and the μ_i are named "modal participation factors". In [9], the aforementioned decomposition utilized the Fourier basis functions, sines and cosines, with good results for closed-form inverse kinematics. However, in this paper the object under consideration, $\dot{\beta}_T(s)$, is discontinuous and would require an extremely high number of Fourier coefficients to decompose accurately; also, a Fourier basis set does not capture any physical meaning for the manipulators considered in this work. Mapping those coefficients back to the μ_i necessary for actuator control would present an additional difficult problem.

However, the natural basis functions are not unique. We now consider the utility of an alternate choice, known as a "wavelet" basis family. The natural basis functions, being "boxes" of finite extent, each support only one section of a multi-section planar robot. In other words, the basis functions have well-defined spatial range, but very limited capacity to affect the entire robot's shape. The wavelet basis to be illustrated next strikes a balance, where certain coefficients may exert influence over the entire robot, while others are more spatially limited for finer detail. This concept is known as "multi-resolution", and has been extensively studied in wavelet theory [17]. Slightly modified for our purposes, the basic wavelet decomposition is

$$\dot{\beta}_T(s) = a_T\varphi(s) + \sum_{j=0}^{J}\sum_{k=0}^{2^j-1} a_{jk}\psi_{jk}(s) \qquad (16)$$

where a_T and a_{jk} are real-valued scale factors. The function $\varphi(s)$ is known as the scaling function, and the family $\psi_{jk}(s)$ are the wavelets. The defining equation in wavelet theory, known as the "dilation equation", defines how the scaling function must behave:

$$\varphi(s) = \sqrt{2}\sum_{k=0}^{N} h_1(k)\varphi(2s-k) \qquad (17)$$

Further, a "mother wavelet" $\psi(s)$ relates to the scaling function as

$$\psi(s) = \sqrt{2}\sum_{k=0}^{N} h_2(k)\varphi(2s-k) \qquad (18)$$

which gives rise to the wavelet family

$$\psi_{jk}(s) = 2^{j/2}\psi(2^j s - k). \qquad (19)$$

The exact sequences $h_1(k)$ and $h_2(k)$, as well as N, determine the behavior of the wavelet family in a fashion much too lengthy to describe here [17]. Suffice it to say that $h_1 = \{1/\sqrt{2}, 1/\sqrt{2}\}$ and $h_2 = \{1/\sqrt{2}, -1/\sqrt{2}\}$ yields a box function for $\varphi(s)$ of unit height, for $s \in [0,1]$, making $\psi_{jk}(s)$ into the concatenation of an "up box" and a "down box". This is known as the Haar wavelet family. The coefficient a_T simply represents the average amplitude of $\dot{\beta}_T$ over the entire range. In (16), the upper summation limit J decides the resolution of the decomposition. For instance, an 8-section planar robot would have 8 degrees of freedom, $\mu_1 ... \mu_8$. Thus we would want to decompose $\dot{\beta}_T(s)$ into 8 coefficients, $\{a_T, a_{00}, a_{10}, a_{11}, a_{20}, a_{21}, a_{22}, a_{23}\}$. Coefficients a_T and a_{00} affect the entire function $\dot{\beta}_T(s)$, while subsequent coefficients limit their effects to smaller and smaller portions of the function. Thus, via multiresolution, by tuning the correct coefficient one may exert influence over a particular localized section of the robot, or the whole robot if desired.

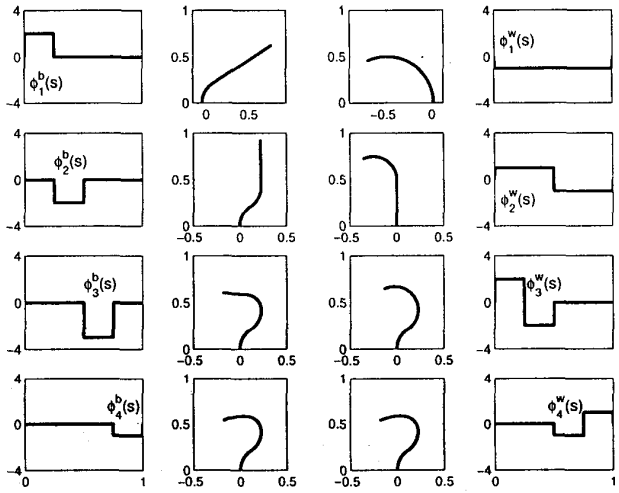

Figure 6: In the center columns, a 4-section continuum robot bends into a "hook" shape. On the left and right are the cumulative effects of synthesizing that shape from natural and wavelet basis functions, respectively. The functions are scaled according to the coefficients $\{\mu_1, \mu_2, \mu_3, \mu_4\}$ and $\{a_T, a_{00}, a_{10}, a_{11}\}$.

If we arrange the coefficients in ascending order of the subscripts, we may write the wavelet decomposition as

$$\dot{\beta}_T(s) = \begin{bmatrix} a_T & a_{00} & \cdots & a_{JK} \end{bmatrix} \begin{bmatrix} \varphi(s) \\ \psi_{00}(s) \\ \vdots \\ \psi_{JK}(s) \end{bmatrix} \triangleq \underline{a}^T \underline{\phi}^w(s) \qquad (20)$$

and, letting $\Phi_i^w(s) = \int_0^1 \phi_i^w(\sigma)d\sigma$, we have

$$\beta_T(s) = \sum_{i=1}^{n} a_i \Phi_i^w(s). \qquad (21)$$

Note that (20) and (21) have the same form as (12) and (14) respectively. Once again, we have projected the func-

tion $\dot{\beta}_T(s)$ (or $\beta_T(s)$) onto a finite-dimensional space, this time using a wavelet basis set rather than the natural basis set. Figure 6 illustrates how we may construct any particular manipulator shape with either choice of basis sets.

6 Redundancy Resolution

The question of redundant robots naturally arises in this context, in order to avoid obstacles or accomplish other subtasks for which a highly redundant continuum robot may be especially well-suited. Consider, for example, asking the n-section planar robot to move its end-effector while attempting to minimize the required amount of bending. The "spring energy" for the continuum planar robot ([3], [10]) is

$$SE = \int_0^1 \frac{1}{2} \left\{ \dot{\beta}_T(s) \right\}^2 ds. \tag{22}$$

Substituting (20) into (22), we find that $\left\{ \dot{\beta}_T(s) \right\}^2 = \underline{a}^T \left[\underline{\phi}^w(s) \right] \left[\underline{\phi}^w(s) \right]^T \underline{a}$. However, for both the natural basis and the Haar wavelet basis, the basis functions $\phi_i(s)$ are orthonormal in the sense of an appropriate inner product. Therefore, $\int_0^1 \underline{\phi}^w(s) \underline{\phi}^w(s)^T ds = I_{n \times n}$ and

$$SE = \int_0^1 \frac{1}{2} \left\{ \dot{\beta}_T(s) \right\}^2 ds = \frac{1}{2} \underline{a}^T \underline{a}. \tag{23}$$

The associated gradient pointing in the direction of minimum bending would be

$$-\nabla_{\underline{a}}(SE) = -\underline{a}. \tag{24}$$

Now we can derive the velocity kinematics, so that

$$\frac{d\underline{x}(s)}{dt} = \frac{d\underline{x}(s)}{d\underline{a}} \frac{d\underline{a}}{dt} \triangleq \left[J(\underline{a}, s) \right] \frac{d\underline{a}}{dt} \tag{25}$$

and observe that the motion executing local minimum-bending behavior is

$$\frac{d\underline{a}}{dt} = \left[J^+ \right] \frac{d\underline{x}(1)}{dt} + k \left[I_{n \times n} - J^+ J \right] \underline{a} \tag{26}$$

where k adjusts how strongly the robot will tend toward the minimum-bending solution. The same expression holds substituting $\underline{\mu}$ for $\underline{a}$. This is reminiscent of the early attempts at joint-limit avoidance for traditional robots, and it hints that we may be able to use much of the vast array of literature on generalized inverses and nullspace projection methods already developed in robotics.

7 Transformations Between Basis Spaces

The next issue of interest concerns the process of mapping the wavelet coefficients back into useful parameters which indicate how to control the robot's actuators. The elements of $\underline{a}$ have little inherent physical meaning at the actuator level, as opposed to the elements of the natural basis set $\underline{\mu}$. We need a transformation from one basis to the other for relating $\underline{a}$ to $\underline{\mu}$.

For distinction, let us denote the natural basis set as $\phi_i^b(s)$ and the wavelet basis set as $\phi_i^w(s)$. Recall that $\beta_T(s) = \underline{a}^T \underline{\phi}^w(s)$ and $\beta_T(s) = \frac{1}{\sqrt{n}} \underline{\mu}^T \underline{\phi}^b(s)$. Since both sets of basis functions are orthonormal, the coefficients are given by inner products $a_i = \left\langle \dot{\beta}_T, \phi_i^w \right\rangle$, and $\mu_i = \sqrt{n} \left\langle \dot{\beta}_T, \phi_i^b \right\rangle$. Combining expressions we find

$$\begin{aligned} \mu_i &= \sqrt{n} \left\langle \underline{a}^T \underline{\phi}^w(s), \phi_i^b(s) \right\rangle = \sqrt{n} \int_0^1 \underline{a}^T \underline{\phi}^w(s) \phi_i^b(s) ds \\ &= \sqrt{n} \sum_{j=1}^{n} a_j \left\{ \int_0^1 \phi_j^w(s) \phi_i^b(s) ds \right\} \end{aligned} \tag{27}$$

which, in matrix form, reads

$$\underline{\mu} = T \underline{a}; \qquad T_{i,j} = \sqrt{n} \int_0^1 \phi_i^b(s) \phi_j^w(s) ds. \tag{28}$$

Referring back to the definitions of $\phi_i^b(s)$ in (13), and $\phi_j^w(s)$ in (17) and (19), an example calculation of T for a 4-section robot (4-DOF in the plane) yields

$$T = 2 \begin{bmatrix} r^2 & r^2 & r & 0 \\ r^2 & r^2 & -r & 0 \\ r^2 & -r^2 & 0 & r \\ r^2 & -r^2 & 0 & -r \end{bmatrix}, \qquad r = \frac{1}{\sqrt{2}}. \tag{29}$$

Since T is unitary, it is a trivial matter to switch back and forth from the natural basis set to the wavelet basis set. Again, one may choose to reduce the dimensionality of the wavelet-based Jacobian by dropping the last k columns ($k \leq n - m$ where n is the DOF of the robot and m is the taskspace dimension), so that $\underline{a} \in \Re^{n-k}$. Now, to return to the natural basis coefficients we use a reduced transformation $T_1 \in \Re^{n \times (n-k)}$ by dropping the last k columns of T. In this manner $\underline{\mu} = T_1 \underline{a}$ and we can then extract the necessary tendon lengths to achieve the desired motion. From an algorithmic point of view, it is noteworthy that T is the matrix-vector equivalent of the Fast Wavelet Transform (FWT) which operates in $O(n)$ complexity.

It is interesting to explore the synergy between these two spaces, namely the natural basis space and the wavelet basis space. Assuming an n-section redundant planar robot, $n > 2$, if we choose the natural basis and only end-effector coordinates matter, then the Jacobian has dimension $J \in \Re^{2 \times n}$. We have already seen how to utilize a generalized inverse, such as the pseudoinverse of J, to obtain how the transform coefficients $\underline{\mu} \in \Re^n$ behave with time. With the wavelet basis, we may simply drop the columns of J which correspond to the finer detail (high resolution) coefficients, until J is square. Multiresolution allows us to explicitly choose how much of the

robot's capability to use without resorting to a generalized inverse but while still maintaining some degree of control over the entire manipulator. This is known as a semi-inverse; specifically, if

$$\frac{d\underline{x}}{dt} = \begin{bmatrix} J_1 & J_2 \end{bmatrix} \frac{d}{dt} \begin{bmatrix} \underline{a}_1 \\ \underline{a}_2 \end{bmatrix}; \qquad J_1 \in \Re^{2\times 2} \tag{30}$$

then we may utilize a semi-inverse to obtain

$$\frac{d\underline{a}}{dt} = \begin{bmatrix} J_1^{-1} \\ 0 \end{bmatrix} \frac{d\underline{x}}{dt} + \begin{bmatrix} -J_1^{-1} J_2 \frac{d}{dt}(\underline{a}_2) \\ \frac{d}{dt}(\underline{a}_2) \end{bmatrix}. \tag{31}$$

The last $n-2$ equations in (31) are trivial identities. However, if we use the fact that $\underline{\mu} = T\underline{a}$, and

$$\underline{\mu} = \begin{bmatrix} T_1 & T_2 \end{bmatrix} \begin{bmatrix} \underline{a}_1 \\ \underline{a}_2 \end{bmatrix} \Rightarrow \begin{bmatrix} \underline{a}_1 \\ \underline{a}_2 \end{bmatrix} = \frac{1}{n} \begin{bmatrix} T_1^T \\ T_2^T \end{bmatrix} \underline{\mu} \tag{32}$$

then we may rewrite (31) as

$$\frac{d\underline{a}}{dt} = \begin{bmatrix} J_1^{-1} \\ 0 \end{bmatrix} \frac{d\underline{x}}{dt} + \begin{bmatrix} -J_1^{-1} J_2 T_2^T \\ T_2^T \end{bmatrix} \underline{\varepsilon}. \tag{33}$$

(where $\underline{\varepsilon} = \frac{1}{n}\frac{d\underline{\mu}}{dt}$). As $\underline{\varepsilon} \in \Re^n$, it plays a role very similar to the gradient in a null-space projection.

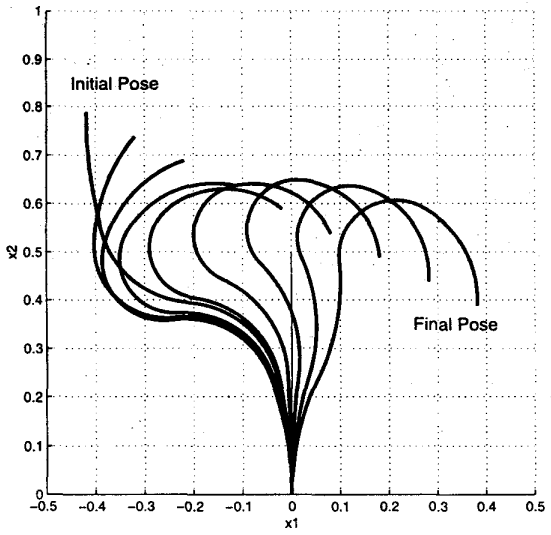

Figure 7: The 4-section manipulator executes a linear trajectory using semi-inverse method. The intial wavelet coefficients are $\underline{a} = \{0, -3, 1, 1\}$.

Non-zero components in $\underline{\varepsilon}$ nudge the appropriate section of the manipulator into motion, while the rest of the wavelet coefficients adjust to automatically position the end-effector on the correct trajectory. In other words, with $\underline{\varepsilon} = 0$, the manipulator moves with broad, low-DOF motions. As necessary, higher-detail localized motions are possible by "turning on" certain elements in $\underline{\varepsilon}$, much like the null-space projection method with a pseudoinverse. In fact, if $\underline{\varepsilon} = -k\underline{\mu}$ for a multi-section manipulator, the self-motion again tends toward minimum-bending configurations. In figure 7, a 4-section continuum robot executes a linear trajectory utilizing the semi-inverse method of (33) with $\underline{\varepsilon} = 0$; in figure 8 the manipulator executes a self-motion with $\frac{d\underline{x}}{dt} = 0$ and $\underline{\varepsilon} = -k\underline{\mu}$. These interesting observations are implicitly made possible by multi-resolution, the property of orthonormality, and the unitary, isometric transformation between the two basis spaces. In the future it may be possible to harness (33) for obstacle avoidance or other useful tasks without the expensive computation of a pseudoinverse.

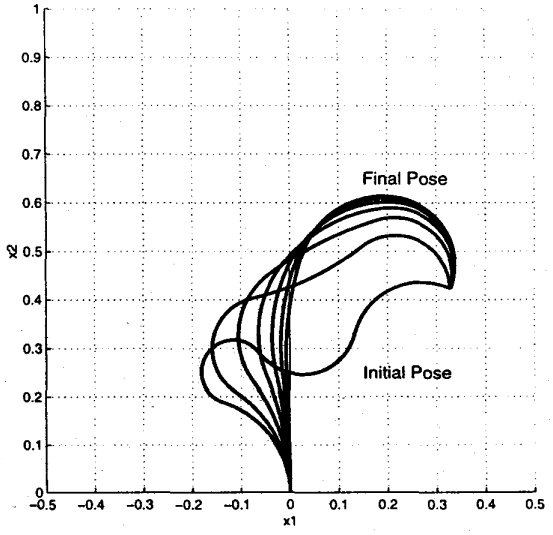

Figure 8: A 4-section continuum robot executes a minimum-bending self-motion using the semi-inverse method. The initial wavelet coefficients are $\underline{a} = \{2, 3, -5, -4\}$

8 Conclusions and Future Work

In this paper, we have discussed some of the basic properties of tendon-driven continuum robots (or robots with a very high backbone DOF which permits them to behave like a continuum robot). We closely examined the velocity kinematics for a redundant planar continuum robot, illustrating two possibilities for the non-unique choice of mappings between the robot's curvature functions and its actuators, using natural and wavelet decompositions. It is hoped that these methods and observations will provide practical and usable tools in the effort to continue the study of remotely-actuated continuum manipulators.

Many problems remain to be solved, however. We have not performed any analysis of the effects of static and dynamic friction on the cables as they travel through the pass-through segments. These effects do alter the shape of

the backbone, especially as the curvature becomes large. Friction effects would impose constraints on the system in (3). Even without constraints, (3) represents a challenge in and of itself. It is a nonlinear system of ODE's with a singularity. This is different from (and in many ways more difficult than) a singular system, for which a significant body of theory exists. As such, even numerical techniques for solving (3) are scant, and one must be very careful to examine the stability of a numerical solution before relying too heavily on its results. Throughout the analysis, we made the assumption that the out-of-plane bending for any given section would not be too large; further work may help reveal how to better account for significant out-of-plane bending. Also, it is unclear whether any parallel exists between the analysis for the planar redundant robots, and general 3-dimensional continuum robots. The transition from 2-dimensional to 3-dimensional spatial analysis appears much more difficult than for traditional rigid-link robots.

Furthermore, the construction of continuum robots presents a number of challenges. While prototypes such as the Elephant's Trunk represent a first step, it defeats some of the possible benefits because it is very heavy. Our ongoing and future work involves the study and creation of newer versions of continuum tendon-driven robots, as well as further examination of the practical and theoretical challenges outlined above.

The authors gratefully acknowledge the support of NSF grant CMS-9796328, DOE contract DE-FG07-97ER1483, and NSF/EPSCoR grant EPS-9630167; thanks to Brian Bunnell and Michael Hannan.

References

[1] S. Hirose, *Biologically Inspired Robots.* Oxford University Press, 1993

[2] I.D. Walker and M.W. Hannan, "A Novel Elephant's Trunk Robot", IEEE/ASME Intl. Conf. on Advanced Intelligent Mechatronics, Atlanta, GA, Sept. 1999, pp. 410-415

[3] I. Gravagne and I.D. Walker, "On the Kinematics of Remotely-Actuated Continuum Robots," IEEE Int'l Conf. on Robotics and Automation (ICRA), San Fransisco, May 2000.

[4] GreyPilgrim company, http://www.greypilgrim.com

[5] R. Cieslak and A. Morecki, "Elephant Trunk Type Elastic Manipulator - a Tool for Bulk and Liquid Materials Transportation," Robotica, 1999, Vol. 17 pp. 11-16

[6] H. Mochiyama and H. Kobayashi, "The Shape Jacobian of a Manipulator with Hyper Degrees of Freedom," Proceedings 1999 IEEE Int'l Conf. on Robotics and Automation (ICRA), Detroit MI, May 1999, pp. 2837-2842

[7] H. Mochiyama and H. Kobayashi, "Shape Correspondence between a Spatial Curve and a Manipulator with Hyper Degrees of Freedom," Proceedings 1998 IEEE/RSJ Int'l Conf. on Intelligent Robots and Systems, Victoria, Canada, October 1998, pp. 161-166

[8] H. Mochiyama, E. Shimemura and H. Kobayashi, "Direct Kinematics of Manipulators with Hyper Degrees of Freedom and Serret-Frenet Formula," Proceedings 1998 IEEE Int. Conf. Robotics and Automation, Leuven, Belgium, May 1998, pp. 1653-1658

[9] G.S. Chirikjian and J.W. Burdick, "A Modal Approach to Hyper-Redundant Manipulator Kinematics," IEEE Transactions on Robotics and Automation, vol. 10, no. 3, June 1994, pp. 343-353

[10] G.S. Chirikjian and J.W. Burdick, "Kinematically Optimal Hyper-Redundant Manipulator Configurations," IEEE Trans. Robotics and Automation, vol. 11, no. 6, Dec 1995, pp. 794-80

[11] G.S. Chirikjian, "A General Numerical Method for Hyper-Redundant Manipulator Inverse Kinematics," Proc. IEEE Int. Conf. Robotics and Automation, Atlanta GA, May 1993, pp. 107-112

[12] G.S. Chirikjian and J.W. Burdick, "Kinematically Optimal Hyper-Redundant Manipulator Configurations," Proc. IEEE Int. Conf. Robotics and Automation, Nice, France, May 1992, pp. 415-420

[13] G.S. Chirikjian and J.W. Burdick, "An Obstacle Avoidance Algorithm for Hyper-Redundant Manipulators," Proc. IEEE Int. Conf. Robotics and Automation, Cincinatti, OH, May 1990, pp. 625-631

[14] G.S. Chirikjian, "Theory and Applications of Hyper-Redundant Robotic Manipulators," Ph.D. thesis, Dept. of Applied Mechanics, California Institute of Technology, June, 1992

[15] G. Robinson and J.B.C. Davies, "Continuum Robots – A State of the Art," Proc. IEEE Int. Conf. Robotics and Automation, Detroit, MI, May 1999, pp. 2849-2854

[16] K. Suzumori, S. Ilkura, and H. Tanaka, "Development of Flexible Microactuator and Its Applications to Robotic Mechanisms," Proc IEEE Int. Conf. Robotics and Automation, Sacramento, CA, April 1991. pp. 1622-1627

[17] C.S. Burrus, R.A. Gopinath, and H. Guo, "Introduction to Wavelets and Wavelet Transforms," Prentice Hall, NJ, 1998

[18] M.W. Spong and M. Vidyasagar, *Robot Dynamics and Control*, John Wiley & Sons, 1989